Biomarker Attenuation Following Virtual Resection Validates Clinically Defined Epileptogenic Networks

Daniel Wang[1,2*], Emily A. Pereira[3], Golnoosh Kamali[1,2], Kristin M. Gunnarsdottir[1,2], Varina Boerwinkle[4], Jorge Gonzalez-Martinez[5], Joon-Yi Kang[6], Sridevi V. Sarma[1,2,6]

[1]Department of Biomedical Engineering, Johns Hopkins University, Baltimore, MD, USA.
[2]Institute for Computational Medicine, Johns Hopkins University, Baltimore, MD, USA.
[3]Department of Electrical and Computer Engineering, Texas Tech University, Lubbock, TX, USA.
[4]Department of Neurology, University of North Carolina School of Medicine, Chapel Hill, NC, USA.
[5]Department of Neurological Surgery, University of Pittsburgh Epilepsy Center, Pittsburgh, PA, USA.
[6]Department of Neurology, Johns Hopkins University, Baltimore, MD, USA.

*Corresponding author(s). E-mail(s): dwang118@jhu.edu;

Abstract

Patients with medically refractory epilepsy who fail antiseizure medications may undergo surgical resection of the epileptogenic zone (EZ), yet postoperative outcomes remain highly variable, with only 30–70% achieving long-term seizure freedom. Computational virtual resection—the simulation of removing candidate brain regions from patient-specific network models—offers a principled framework for evaluating proposed surgical plans prior to intervention. Because clinically defined EZs are hypothesis-driven and may be incomplete or incorrect, an objective test of their network impact is critically needed. Here, we assess the leading eigenvector (LEV) of dynamic network models (DNMs), derived from intracranial EEG (iEEG), as a biomarker for virtual resection efficacy. Using iEEG recordings from 44 patients across four epilepsy centers, we constructed

DNMs and quantified LEV components before and after virtual resection of clinically annotated EZ channels. Attenuation of EZ-associated LEV components following virtual resection distinguished favorable (Engel Class 1) from unfavorable (Engel Class 2–4) surgical outcomes, achieving an area under the curve of 0.8, with 71% accuracy, 74% specificity, and 67% sensitivity. These results establish LEV attenuation as a computational biomarker for evaluating clinically defined epileptogenic network hypotheses and suggest that LEV-based virtual resection may inform patient-specific surgical decision-making.

Keywords: epilepsy, virtual resection, dynamic network models, leading eigenvector, interictal biomarker, epileptogenic zone, surgical outcome

1 Introduction

Epilepsy is a chronic neurological disorder characterized by recurrent, unprovoked seizures that affects over 60 million people worldwide [1]. Approximately one-third of individuals with epilepsy suffer from medically refractory epilepsy (MRE), defined as inadequate seizure control despite treatment with two or more appropriately chosen antiseizure medications [2–5]. For these patients, surgical resection of the epileptogenic zone (EZ), which comprises specific brain region(s) necessary and sufficient for initiating seizures and whose removal (or disconnection) results in complete abolition of seizures [6]. However, surgical outcomes remain highly variable, with only 30-70% of patients achieving long-term seizure freedom, largely due to challenges in accurately localizing the EZ [7–9].

Presurgical evaluation of MRE often requires prolonged inpatient monitoring with invasive intracranial EEG (iEEG), during which clinicians await spontaneous seizures to visually identify early ictal (seizure) electrographic changes that delineate the EZ [7, 10, 11]. This process is time-consuming, costly, and increases patient risk due to extended electrode implantation. In contrast, interictal (between seizure) recordings are abundant and safer to acquire, motivating efforts to identify interictal biomarkers of the EZ. High-frequency oscillations (HFOs) have been proposed for this purpose, but their clinical utility has been limited by inconsistent performance, challenges in distinguishing pathological from physiological HFOs, and channel-wise analyses that fail to capture network-level dynamics [12–14].

Network-based computational approaches have emerged as a promising framework for understanding epilepsy as a disorder of brain connectivity rather than focal pathology [15]. Patient-specific dynamic network models (DNMs) can be estimated from short iEEG recordings to capture directional influences among brain regions [16]. This framework enables the development of network-level biomarkers reflecting the underlying dynamical properties of the epileptic brain. The source-sink index (SSI), which quantifies the extent to which certain nodes are persistently inhibited by other network regions during interictal periods, has shown improved predictive performance for surgical outcomes compared to HFOs [17]. More recently, the leading eigenvector (LEV) of the DNM state-transition matrix has been proposed as a theoretically principled

biomarker that is highly correlated with the SSI [18]. In linear systems theory, the LEV represents the steady-state distribution of network activity, with nodes exhibiting high LEV components corresponding to network sinks that accumulate influence from other regions [19].

Virtual resection—the computational simulation of removing candidate brain regions from patient-specific models—has emerged as a promising framework for evaluating surgical hypotheses prior to intervention [20–25]. By simulating the removal of specific brain regions in patient-specific computational models, virtual resection enables testing of different surgical hypotheses before actual intervention. Prior work has shown that virtual resection strategies can, in principle, predict surgical outcomes or identify optimal resection targets. However, existing approaches have relied on small, single-center cohorts [20], required ictal or peri-ictal data [20], involved computationally intensive neural mass models with extensive parameter tuning [26], or depended on specialized neuroimaging modalities such as diffusion MRI [27]. Other studies have focused primarily on optimizing resection extent rather than predicting clinical outcome [21], or have been validated largely in simulation or narrowly defined patient populations [24]. Collectively, these limitations have hindered translation of virtual resection methods into routine clinical decision-making.

demonstrated that synchronizability-based virtual resection could predict surgical outcomes with an AUC of 0.89, reporting that removal of synchronizing brain regions was associated with improved clinical outcomes [20]. However, their approach relied on a single-center cohort of 28 patients from the University of Pennsylvania and required functional connectivity estimates derived from both pre-ictal and ictal recordings, limiting applicability in clinical settings where waiting for seizures prolongs invasive monitoring. While recent work has demonstrated the potential of computational modeling, neural mass models require extensive parameter tuning and are computationally intensive [26]. however, this approach requires specialized neuroimaging infrastructure and computational resources that may limit widespread clinical adoption. Nissen et al. demonstrated that optimized virtual resections on individual structural brain networks could achieve effects comparable to actual surgery while sparing on average 27.5% of tissue, though their study of 19 patients focused primarily on optimizing resection extent rather than predicting surgical outcomes [21]. Other studies have been limited by small sample sizes, Li et al. analyzed only 16 patients using autoregressive connectivity networks [23], while Sun et al. validated their sEEG propagation network approach on limited clinical data [25]. Kalitzin et al. validated their virtual resection paradigm primarily on computational simulations rather than clinical outcomes [24]. Demuru et al. restricted their analysis to 11 patients with extra-temporal focal epilepsy and concluded from their validation study that virtual resection methods "are not yet mature to inform clinical decision-making" [22].

While interictal network biomarkers such as the SSI and LEV can characterize clinically defined EZs, their utility for virtual resection—specifically, whether biomarker changes induced by simulated resection predict actual surgical outcomes—remains unexplored. Establishing this link is essential for transforming network-based biomarkers into actionable tools for presurgical evaluation. Here, we test the hypothesis that

attenuation of EZ-associated LEV components following virtual resection of clinically annotated regions predicts surgical outcome. Using iEEG data from 44 MRE patients across four epilepsy centers, we constructed patient-specific DNMs and quantified LEV components before and after simulated resection. We show that LEV-based virtual resection achieves clinically meaningful predictive accuracy, validating LEV attenuation as a computational biomarker for evaluating proposed surgical plans and informing patient-specific epilepsy surgery.

2 Results

2.1 Virtual Resection Produces Differential LEV Changes in Successful versus Failed Surgical Outcomes

To evaluate the utility of the leading eigenvector (LEV) as a biomarker for virtual resection, we examined the distribution of LEV changes across patients following simulated removal of clinically annotated epileptogenic zone (EZ) channels. For each iEEG channel, we computed $\Delta\text{LEV} = |\text{LEV}_{pre}| - |\text{LEV}_{post}|$, which quantifies the change in LEV magnitude induced by virtual resection. Positive values indicate attenuation of network influence following simulated EZ removal (Figure 1).

Distinct distributional patterns emerged that corresponded to surgical outcome. In patients who achieved seizure freedom (Engel Class 1), EZ channels were disproportionately represented in the upper tail of the ΔLEV distribution. For example, patient UPMC6 exhibited an EZ tail proportion of 0.784, indicating that virtual resection produced large LEV reductions primarily within EZ-labeled regions (Figure 2). This pattern is consistent with the hypothesis that successful resections target network elements exerting strong influence on interictal dynamics, such that their removal substantially alters the network's steady-state behavior.

In contrast, patients with unfavorable surgical outcomes showed markedly lower EZ representation in the distribution tail. Patient NIH9 (Engel Class 3) exhibited an EZ tail proportion of 0.175, while patient LA15 (Engel Class 4) showed a value of 0.078. In these cases, virtual resection of clinically identified EZ channels produced minimal changes in LEV magnitude, suggesting that the annotated EZ either incompletely captured the true epileptogenic network or omitted additional regions critical to seizure generation.

Kernel density estimates overlaid on the ΔLEV histograms (Figure 2) revealed that the overall shape of the distributions was broadly similar across patients. The primary distinguishing feature was the composition of extreme values rather than global distributional differences. This observation supports the use of tail-based metrics as a standardized measure across patients and recording conditions. Complete ΔLEV distributions for all 44 patients are provided in Supplementary Figures S1–S4.

2.2 EZ Tail Proportion Differentiates Surgical Outcome Groups

We next asked whether the proportion of EZ channels in the upper tail of the ΔLEV distribution could serve as a patient-level predictor of surgical outcome. For each

patient, we computed the fraction of channels within the top 5% of ΔLEV values that originated from clinically annotated EZ regions, hereafter referred to as the "EZ tail proportion".

Patients achieving Engel Class 1 outcomes ($n = 21$) exhibited substantially higher EZ tail proportions than those with Engel Class 2–4 outcomes ($n = 23$) (Figure 3). Logistic regression confirmed a significant association between EZ tail proportion and surgical outcome (likelihood ratio test, $p = 4.49 \times 10^{-5}$). Leave-one-out cross-validation demonstrated robust predictive performance with an accuracy of 71% and an area under the receiver operating characteristic curve (AUC) of 0.8. These results reflect the central premise of our approach: when the clinically defined EZ accurately captures the epileptogenic network, virtual resection induces large ΔLEV reductions concentrated within EZ channels. These findings support the EZ tail proportion as a candidate biomarker linking virtual resection to clinical outcome.

2.3 LEV-Based Virtual Resection Enables Clinically Meaningful Outcome Prediction

To formally assess predictive performance, we trained a logistic regression classifier using EZ tail proportion as the sole predictor for binary surgical outcome (Engel Class 1 versus Engel Class 2–4). Model performance was evaluated using leave-one-out cross-validation across all 44 patients (21 Engel Class 1; 23 Engel Class 2–4), with each patient iteratively held out for testing while the model was trained on the remaining cohort.

The classifier achieved robust and consistent performance across folds. On the held-out test cases, the model yielded an area under the receiver operating characteristic curve (AUC) of 0.8, with 71% accuracy, 74% specificity, and 67% sensitivity (Figure 4). The receiver operating characteristic curve demonstrated stable discrimination across a range of decision thresholds. Analysis of model coefficients confirmed the statistical significance of EZ tail proportion as a predictor ($p = 0.0014$; Table 2). The positive standardized coefficient indicates that higher EZ tail proportion values are associated with increased likelihood of seizure freedom, with each unit increase corresponding to approximately a 1.5-fold increase in the odds of achieving an Engel Class 1 outcome.

The resulting confusion matrix revealed six false-positive predictions (predicted Engel Class 1, observed Engel Class 2–4) and seven false-negative predictions (predicted Engel Class 2–4, observed Engel Class 1), highlighting clinically interpretable error modes and underscoring the model's role as a decision-support tool rather than a deterministic predictor.

2.4 LEV Performance is Invariant to Demographic and Clinical Characteristics

To assess the clinical generalizability of the LEV-based EZ localization metric, we evaluated whether the EZ tail proportion was confounded by demographic or clinical factors unrelated to surgical outcome. Following previously established methodology for assessing biomarker invariance [16], we computed Cohen's d effect sizes with

95% bootstrap confidence intervals and performed non-parametric group comparisons across key clinical covariates (Figure 5).

No significant difference in EZ tail proportion was observed between male ($n = 23$; mean±SD: 0.318 ± 0.206) and female ($n = 20$; mean±SD: 0.330 ± 0.224) patients (Mann-Whitney U test, $p = 0.894$). The effect size was negligible (Cohen's $d = -0.057$; 95% CI: $[-0.674, 0.561]$), indicating that LEV-based EZ localization is invariant to patient sex (Figure 5A,F).

Patients with MRI-positive lesional epilepsy ($n = 12$; mean±SD: 0.316 ± 0.139) and MRI-negative nonlesional epilepsy ($n = 31$; mean±SD: 0.327 ± 0.238) exhibited comparable EZ tail proportion distributions (Mann-Whitney U test, $p = 0.797$). The negligible effect size (Cohen's $d = -0.051$; 95% CI: $[-0.738, 0.635]$) confirms that the LEV metric is equally effective for both lesional and nonlesional cases (Figure 5C,F). This finding is particularly clinically relevant, as nonlesional epilepsy cases represent a challenging population where traditional imaging-based EZ localization often fails.

Comparison between temporal lobe epilepsy ($n = 5$; mean±SD: 0.409 ± 0.189) and extra-temporal epilepsy ($n = 26$; mean±SD: 0.320 ± 0.200) revealed a small effect size (Cohen's $d = 0.431$; 95% CI: $[-0.574, 1.436]$) that did not reach statistical significance (Mann-Whitney U test, $p = 0.658$). While the wide confidence interval reflects the limited temporal lobe sample size, the non-significant difference suggests the LEV metric performs consistently across different epileptogenic network topologies (Figure 5D,F).

Across four independent clinical centers (CC, JHU, NIH, UPMC), no significant overall difference in EZ tail proportion was detected (Kruskal-Wallis test, $H = 1.447$, $p = 0.695$). However, the maximum pairwise effect size between centers (CC vs. UPMC: Cohen's $d = 0.546$) fell within the medium effect range, suggesting modest inter-center variability (Figure 5B,E). Importantly, despite this variability, the separation between good (Engel I) and poor (Engel II+) surgical outcomes remained consistent across all centers (Figure 5E), with Engel I patients consistently demonstrating higher EZ tail proportions than Engel II+ patients at each site. This pattern indicates that while absolute EZ tail proportion values may vary slightly by center—potentially reflecting differences in electrode placement protocols, data acquisition systems, or patient selection criteria—the relative discriminative capacity of the LEV metric is preserved.

As a positive control, we confirmed that surgical outcome itself produced a large effect on EZ tail proportion, as expected if the metric captures clinically meaningful information. Engel I patients ($n = 21$; mean±SD: 0.449 ± 0.194) exhibited significantly higher EZ tail proportions than Engel II+ patients ($n = 23$; mean±SD: 0.206 ± 0.155; Mann-Whitney U test, $p < 0.001$). The large effect size (Cohen's $d = 1.36$; 95% CI: $[0.684, 2.036]$) validates that the LEV-based metric captures variance specifically associated with surgical outcome rather than demographic or clinical confounders (Figure 5F).

Taken together, these results demonstrate that LEV-based EZ localization is robust to patient sex and MRI lesional status (negligible effects, $|d| < 0.2$), with modest sensitivity to epilepsy localization type ($|d| = 0.43$) and medical center ($|d| = 0.55$). Critically, the large effect size for surgical outcome ($d = 1.36$) relative to demographic

factors confirms that the observed differences in EZ tail proportion reflect true predictive signal rather than systematic bias from clinical covariates. These findings support the generalizability of the LEV biomarker across heterogeneous patient populations and clinical settings.

3 Discussion

In this study, we evaluated the leading eigenvector (LEV) of patient-specific dynamic network models as a biomarker for virtual resection, that is the computational testing of proposed surgical plans, in drug-resistant epilepsy. We show that attenuation of EZ-associated LEV components following simulated resection of clinically annotated regions reliably distinguishes favorable from unfavorable surgical outcomes in a multicenter cohort. These findings establish LEV-based virtual resection as a principled, network-level approach for evaluating presurgical hypotheses using interictal data.

3.1 Leading Eigenvector as a Perturbation-Responsive Biomarker

The utility of the LEV as a biomarker is grounded in linear systems theory, where the leading eigenvector reflects the dominant steady-state mode of a dynamical network and captures how activity is distributed across nodes under persistent interactions. In the context of brain networks, the LEV encodes a global hierarchy of influence: nodes with large positive LEV components occupy privileged positions in the network, exerting sustained control over network dynamics, while nodes with smaller components are primarily shaped by incoming influence. As such, the LEV provides a compact, model-derived summary of long-timescale network organization that is not apparent from pairwise connectivity measures alone.

Prior work established that the LEV is closely related to the source–sink index (SSI), an interictal biomarker reflecting the hypothesis that epileptogenic regions are persistently suppressed by surrounding networks between seizures [17]. In this framework, epileptogenic zones occupy sink-like positions in the interictal state, characterized by strong incoming influence and limited outgoing control. The LEV captures this organization naturally: sink-like nodes exhibit elevated LEV magnitude because they are tightly embedded in, and stabilized by, the dominant network mode. Importantly, this interpretation does not rely on transient seizure activity, but instead reflects stable network structure estimated from interictal recordings.

Our results extend this conceptual framework in a critical direction by demonstrating that the LEV is not merely descriptive, but intervention-sensitive. When clinically annotated EZ regions are virtually resected, implemented as targeted removal of nodes or edges from the patient-specific dynamical model, the resulting perturbation propagates through the network and alters its dominant eigenmode. We find that successful surgical plans are characterized by a marked attenuation of EZ-associated LEV components following virtual resection, whereas unsuccessful plans leave the dominant mode largely intact. This distinction suggests that favorable outcomes occur when surgery disrupts the core network structure sustaining pathological dynamics, rather than simply removing regions that are anatomically or visually suspicious.

From a systems perspective, this behavior is expected: the leading eigenvector governs the asymptotic behavior of linear dynamical systems, and perturbations that significantly reduce its magnitude or redistribute its mass correspond to fundamental changes in network stability and control. Thus, LEV attenuation provides a principled, mechanistic criterion for evaluating whether a proposed resection meaningfully alters the pathological network state. Unlike heuristics based on lesion size, spatial overlap, or local connectivity strength, the LEV directly tests whether the hypothesized epileptogenic network has been functionally dismantled.

3.2 Virtual Resection Approaches

Our approach differs from prior virtual resection studies in several important respects. A range of computational frameworks have previously been proposed to evaluate surgical hypotheses, including synchronizability-based metrics derived from functional connectivity [20], neural mass models that assess proximity to ictal bifurcations [26, 27], and approaches that rely on perturbations of structural connectivity inferred from diffusion imaging [21]. These methods have provided valuable insight into seizure generation and propagation, but often require ictal or peri-ictal data, computationally intensive simulations, or multimodal imaging that may not be available or reliable in all clinical settings.

In contrast, our framework operates entirely on interictal iEEG and leverages steady-state properties of patient-specific dynamical network models. Rather than estimating proximity to seizure onset or optimizing network synchronizability, LEV-based virtual resection evaluates whether a proposed intervention disrupts the dominant network mode that stabilizes pathological dynamics between seizures. This distinction is critical: whereas prior approaches often assess whether a network is rendered less seizure-prone in principle, the LEV explicitly tests whether the hypothesized epileptogenic network has been functionally dismantled by the proposed resection.

A further advantage of the LEV framework is its simplicity and interpretability. The proportion of clinically annotated EZ channels in the upper tail of the ΔLEV distribution yields a single scalar metric per patient that can be directly compared across surgical hypotheses. This avoids the need for extensive parameter tuning or model calibration and facilitates integration into clinical workflows. Despite this relative simplicity, predictive performance was comparable to that reported by more complex approaches. For example, Kini et al. reported high predictive accuracy using synchronizability-based virtual resection in a smaller single-center cohort [20], while Goodfellow et al. achieved similar performance using neural mass models and bifurcation analysis [26]. Importantly, our results were validated across a multicenter cohort spanning four epilepsy centers, enhancing generalizability and mitigating center-specific biases that can influence model performance [22]. Together, these findings suggest that steady-state network perturbations captured by the leading eigenvector encode outcome-relevant information that is robust across recording sites and clinical practices, supporting LEV-based virtual resection as a scalable and data-efficient alternative for presurgical evaluation.

3.3 Relevance to Basic and Translational Neuroscience

Beyond its clinical implications, this work has direct relevance to both basic and translational neuroscience by linking dynamical systems theory to experimentally observable brain network organization. At a fundamental level, the leading eigenvector provides a principled representation of how large-scale neural networks self-organize under persistent interactions, capturing a dominant mode that reflects long-timescale stability, hierarchy, and control. Our results demonstrate that this dominant mode is not merely a mathematical abstraction, but corresponds to biologically meaningful structure that constrains pathological brain dynamics in epilepsy.

From a basic neuroscience perspective, the findings support the view that epileptogenic regions are embedded within, and stabilized by, distributed networks during the interictal state, rather than acting as autonomous seizure generators. The sensitivity of the LEV to targeted perturbations provides evidence that seizure propensity is governed by global network organization, offering a mechanistic bridge between cellular-level excitability and systems-level seizure emergence. More broadly, this work illustrates how steady-state network modes can serve as interpretable descriptors of brain function in nonstationary, pathological regimes.

Translationally, the LEV framework exemplifies how mechanistic network models can be leveraged to generate testable, intervention-relevant predictions from human neural recordings. By enabling virtual resection using interictal data, this approach transforms descriptive biomarkers into actionable computational assays, narrowing the gap between theoretical neuroscience and clinical decision-making. The same modeling principles may generalize to other network disorders—including movement disorders, chronic pain, and neuropsychiatric disease—where targeted perturbations aim to reshape maladaptive network states. Together, these results highlight the broader utility of eigenmode-based representations as a unifying language across basic, translational, and clinical neuroscience, demonstrating how abstract systems-level constructs can yield concrete insight into brain dysfunction and its remediation.

3.4 Clinical Impact

More broadly, these findings position the LEV as a bridge between network neuroscience and surgical decision-making. By enabling virtual resection, the in silico testing of competing surgical hypotheses, the LEV framework allows clinicians to ask not only where seizures arise, but whether a planned intervention is sufficient to neutralize the underlying pathological network. This reframes presurgical evaluation from a problem of localization alone to one of mechanism-based validation, grounded in patient-specific network dynamics.

A key clinical advantage of the LEV-based approach is its reliance on interictal data, which are routinely collected and substantially more abundant than seizures in intracranial EEG monitoring. This reduces dependence on capturing representative seizures, shortens monitoring duration, and mitigates risks associated with prolonged invasive recordings. In practice, LEV-based virtual resection could be incorporated

alongside standard presurgical workups to evaluate candidate resections early, providing objective feedback on whether a proposed plan is likely to meaningfully disrupt the epileptogenic network before irreversible intervention.

Importantly, our results suggest that surgical failure may often arise not from incorrect localization per se, but from incomplete disruption of the pathological network. In unsuccessful cases, clinically annotated EZ regions may be removed, yet the dominant network mode, captured by the LEV, remains largely intact. From a clinical standpoint, this offers a quantitative explanation for why anatomically plausible resections sometimes fail and highlights the potential value of expanding, refining, or re-targeting surgical plans to address network-level pathology rather than isolated regions.

The LEV framework may also support comparative evaluation of alternative interventions, including extended resections, staged procedures, or focal neuromodulation strategies. Because the metric explicitly quantifies how proposed perturbations alter the dominant network mode, it provides a common language for assessing the expected impact of diverse treatment options on pathological dynamics. This is particularly relevant in complex cases involving multifocal epilepsy, eloquent cortex, or deep network hubs, where surgical decisions must balance efficacy against functional risk.

Finally, by grounding outcome prediction in interpretable systems-level principles rather than black-box classification, LEV-based virtual resection aligns with the needs of clinical decision-making. The directionality and magnitude of LEV attenuation offer an intuitive measure of whether a hypothesized epileptogenic network has been functionally dismantled, facilitating communication between clinicians, engineers, and patients. Together, these features suggest that LEV-based virtual resection has the potential to enhance surgical planning, reduce failed interventions, and move epilepsy surgery toward a more principled, network-informed paradigm.

3.5 Methodological Considerations and Limitations

Several methodological considerations inform the interpretation of these results. First, the LEV-based virtual resection framework evaluates the impact of perturbing candidate resection plans within the set of brain regions sampled during intracranial monitoring. Within this sampled network, the approach enables systematic comparison of alternative surgical hypotheses and can, in principle, identify resection plans that more effectively disrupt the dominant pathological network mode than the clinically proposed plan. However, the framework is inherently limited by electrode coverage: if critical components of the epileptogenic network are not sampled by the implanted electrodes, virtual resection cannot evaluate or compensate for their omission. Thus, LEV-based virtual resection is well suited for refining and testing surgical strategies within observed networks, but it cannot recover epileptogenic regions that lie outside the monitored cortical and subcortical territory.

Second, the network models used here are estimated from interictal recordings and capture steady-state properties of pathological dynamics. While this design choice enables data-efficient modeling and avoids reliance on seizure capture, it necessarily abstracts away transient ictal mechanisms and nonlinear state transitions that may also contribute to surgical outcome. Thus, LEV-based virtual resection should be viewed as complementary to seizure-based analyses rather than a replacement.

Third, outcome classification was based on seizure status at one year postoperatively. Although this time point is standard in surgical outcome studies, longer follow-up may reveal delayed seizure recurrence, particularly in cases where residual network pathology persists. In addition, the cohort consisted exclusively of patients who proceeded to surgery, introducing potential selection bias that may limit generalizability to earlier stages of presurgical evaluation. Prospective validation applied prior to surgical decision-making will be critical for establishing clinical utility. The observed false-positive and false-negative predictions further reflect these methodological constraints. False positives may arise when the epileptogenic network is correctly identified but cannot be fully resected due to involvement of eloquent cortex, while false negatives may occur when effective resections extend beyond narrowly defined EZ boundaries or when model estimation is limited by sparse sampling. These error modes highlight that LEV-based virtual resection is best interpreted as a decision-support tool that provides quantitative guidance rather than deterministic predictions.

Future work will address these limitations by prospectively evaluating multiple alternative resection hypotheses in silico, integrating multimodal information such as structural connectivity and imaging, and extending the framework to neuromodulation contexts, including responsive neurostimulation. In such settings, identifying network elements whose perturbation maximally attenuates the dominant pathological mode may inform stimulation targeting and adaptive control strategies.

4 Methods

4.1 Experimental Model and Study Participant Details

4.1.1 Human Participants

This retrospective study analyzed 44 adults with medically refractory epilepsy who underwent presurgical evaluation with intracranial stereo-electroencephalography (sEEG) monitoring followed by surgical treatment. Participants ranged in age from 16 to 65 years (mean 31.8 $\pm$ 12.3 years) and included 24 males and 20 females. All participants had at least one year of postoperative follow-up to assess clinical outcomes. Participants were treated across four epilepsy centers: Cleveland Clinic (CC; $n = 27$), Johns Hopkins Hospital (JHH; $n = 4$), National Institutes of Health (NIH; $n = 8$), and University of Pittsburgh Medical Center (UPMC; $n = 5$). Post-iEEG interventions included resective surgery ($n = 29$) or laser ablation ($n = 15$). Of the 44 patients, 21 achieved successful surgical outcomes (Engel Class 1) and 23 had failed outcomes (Engel Class 2–4) at one year postoperatively. Each participating institution obtained approval from their respective Institutional Review Board for retrospective analysis of clinical data. All patients provided informed consent for use of their clinical data in research as part of their clinical care agreements. All methods were performed in accordance with the relevant guidelines and regulations. Detailed demographic and clinical characteristics are summarized in Table 1.

4.1.2 Sex and Gender Considerations

The study cohort included 24 male and 20 female participants. Sex was determined based on clinical records. Given the retrospective nature of the study and the focus on computational biomarker validation, we did not perform sex-stratified analyses. The influence of sex on LEV-based virtual resection metrics represents an important area for future investigation in larger cohorts.

4.2 Stereo-Electroencephalography Recording

Intracranial stereo-EEG (sEEG) data were recorded using Nihon Kohden or Natus (Natus Medical Inc.) EEG monitoring and diagnostic systems. The majority of recordings were acquired at sampling frequencies of 1 or 2 kHz, with a small subset recorded at 500/512 Hz. The clinical team at each center determined electrode placement based on presurgical hypotheses generated from noninvasive evaluation including scalp EEG, neuroimaging, and neuropsychological testing. For each patient, a single randomly selected interictal epoch was extracted, defined as occurring at least one hour away from any recorded seizure event. The mean duration of analyzed epochs was 5.3 ± 4.2 minutes. No specific selection criteria were applied beyond the interictal timing requirement, ensuring that the analysis reflects typical interictal network dynamics rather than periictal states.

4.3 Clinical Annotation of the Epileptogenic Zone

The clinical team at each participating epilepsy center developed an EZ hypothesis for each patient as part of standard presurgical evaluation. The clinically annotated EZ was defined as the anatomical region(s) identified for targeted treatment, including resection, ablation, or stimulation. This annotation was performed prior to surgery based on comprehensive multimodal assessment. The EZ hypothesis included sEEG channels displaying early electrophysiological changes at seizure onset, typically characterized by low-voltage fast activity, as well as channels involved in early seizure propagation. Because surgical treatment is guided by the EZ hypothesis, substantial overlap typically exists between clinically annotated EZ channels and the actual resected or ablated tissue.

4.4 Classification of Surgical Outcomes

Surgical outcomes were classified by each center's epileptologist using the Engel Surgical Outcome Scale at a minimum of 12 months postoperatively. Successful surgical outcomes were defined as Engel Class 1 (free of disabling seizures), while failed outcomes were defined as Engel Class 2–4 (any ongoing disabling seizures). Of the 44 patients in the cohort, 21 (47.7%) achieved successful outcomes and 23 (52.3%) had failed outcomes.

4.5 Signal Preprocessing

Intracranial sEEG recordings were preprocessed using standardized procedures implemented in MATLAB R2020b (MathWorks, Natick, MA). Each signal was bandpass

filtered between 0.5 Hz and 300 Hz using a fourth-order Butterworth filter to retain physiologically relevant frequency content while removing DC offset and high-frequency noise. Power line interference was attenuated by applying notch filters at 60 Hz and its harmonics (120 Hz, 180 Hz, 240 Hz) with a stopband width of 2 Hz. A common average reference was then computed and subtracted from all channels to reduce common-mode noise and reference-related artifacts. Electrode locations were determined by co-registering post-implantation computed tomography (CT) scans with preoperative brain MRI using BioImage Suite software. The clinical team visually verified electrode placement, and channels not recording from gray matter or deemed excessively noisy by clinical review were excluded from analysis. This resulted in 95 $\pm$ 32 (mean $\pm$ SD) sEEG channels per patient included in the final analysis. The preprocessed sEEG recordings were segmented into non-overlapping 500 ms windows for subsequent dynamic network model estimation. This window duration was selected to balance temporal resolution with statistical stability of model parameter estimates.

4.6 Dynamic Network Model Estimation

Dynamic network models (DNMs) were used to characterize directional influences among iEEG channels during interictal periods. The interictal DNM was represented as a linear time-varying (LTV) model comprising a sequence of linear time-invariant (LTI) models estimated from successive 500 ms data windows. For each window, we estimated an LTI model of the form:

$$x(t+1) = Ax(t) \tag{1}$$

where $x(t) \in \mathbb{R}^N$ denotes the vector of iEEG channel amplitudes at discrete time t, and $A \in \mathbb{R}^{N \times N}$ is the state-transition matrix describing the directed influences between channels. Each element A_{ij} quantifies the influence of channel j on channel i at the subsequent time step. This formulation can be viewed as a first-order multivariate autoregressive (MVAR) model, a widely used approach for analyzing effective connectivity in brain networks.

The state-transition matrix A was estimated using ordinary least squares regression. Specifically, for each 500 ms window containing T time samples, we formed the matrices $X_0 = [x(1), x(2), \ldots, x(T-1)]$ and $X_1 = [x(2), x(3), \ldots, x(T)]$, then computed $A = X_1 X_0^T (X_0 X_0^T)^{-1}$. Model quality was assessed using the coefficient of determination (R^2) between predicted and observed signals. Only A matrices achieving $R^2 > 0.6$ were retained for subsequent analysis, ensuring that the estimated network models adequately captured the temporal dynamics of the recorded signals. Model estimation and all subsequent analyses were implemented in Python 3.11 (Python Software Foundation).

4.7 Leading Eigenvector Computation

For each retained state-transition matrix A, we computed the leading eigenvector (LEV), the eigenvector associated with the eigenvalue of largest magnitude. In linear systems theory, the LEV characterizes the dominant mode of system dynamics and

represents the direction along which the system state grows most rapidly (for eigenvalues > 1) or decays most slowly (for eigenvalues < 1). The LEV was computed using standard eigenvalue decomposition algorithms (numpy.linalg.eig in Python). For each channel i, the corresponding LEV component v_i quantifies that channel's participation in the dominant network mode. Channels with high LEV magnitude correspond to network "sinks" that accumulate influence from other regions, consistent with the theoretical interpretation of the source-sink framework.

4.8 Virtual Resection Procedure

Virtual resection was performed by simulating the removal of clinically annotated EZ channels from the network model. Specifically, for each retained A matrix, we created a post-resection matrix A_{post} by setting the columns corresponding to EZ channels to zero:

$$A_{post}(:, j) = 0 \quad \text{for all } j \in \text{EZ} \tag{2}$$

This operation eliminates the outgoing influence of EZ channels on the rest of the network while preserving their incoming connections, modeling the effect of surgical removal on network dynamics. The procedure was applied independently to each A matrix, yielding paired pre-resection and post-resection matrices for each 500 ms window. The LEV was then recomputed for each post-resection matrix A_{post}, yielding LEV_{post}. The change in LEV components was quantified as:

$$\Delta\text{LEV} = |\text{LEV}_{pre}| - |\text{LEV}_{post}| \tag{3}$$

where the absolute value ensures that the metric captures magnitude changes regardless of eigenvector sign ambiguity.

4.9 Feature Extraction

A single patient-level feature was derived from the ΔLEV data to serve as a predictor of surgical outcome. For each patient, all ΔLEV values across time windows and channels were pooled into a single distribution. The high-magnitude tail was defined as the top 5% of values in this distribution, an exploratory threshold selected to capture channels exhibiting the largest changes following virtual resection. We then calculated the proportion of elements in this high-magnitude tail that originated from clinically annotated EZ channels:

$$\text{EZ tail proportion} = \frac{\text{Number of tail elements from EZ channels}}{\text{Total number of tail elements}} \tag{4}$$

This scalar feature quantifies the extent to which virtual resection specifically affects EZ channels relative to non-EZ channels. Higher values indicate that EZ channels disproportionately contribute to large ΔLEV changes, suggesting that the clinical EZ hypothesis captures the network regions most influential in interictal dynamics.

4.10 Quantification and Statistical Analysis

4.10.1 Statistical Comparisons

Differences in EZ tail proportion between surgical outcome groups (Engel Class 1 versus Engel Class 2–4) were assessed using Mann-Whitney U tests, a non-parametric alternative appropriate for non-normally distributed data and modest sample sizes. Significance was defined as $p < 0.05$.

4.10.2 Effect Size Estimation and Invariance Assessment

To evaluate the clinical generalizability of the LEV-based biomarker, we assessed its invariance to demographic and clinical covariates following previously established methodology [16]. Effect sizes were quantified using Cohen's d, with 95% confidence intervals estimated via bootstrap resampling (10,000 iterations). For comparisons across more than two groups (e.g., medical centers), the Kruskal-Wallis H test was employed. Covariates evaluated included patient sex, MRI lesional status (lesional vs. nonlesional), epilepsy localization (temporal vs. extra-temporal), and medical center. As a positive control, we verified that surgical outcome (Engel Class 1 vs. 2+) produced a large effect size, confirming that the metric captures clinically meaningful variance rather than demographic confounders.

4.10.3 Predictive Modeling

Logistic regression was used for binary classification of surgical outcomes. The model was trained using the EZ tail proportion as the sole predictor variable, with standardization (z-scoring) applied prior to model fitting. Model performance was evaluated using multiple metrics: area under the receiver operating characteristic curve (AUC), accuracy, sensitivity (true positive rate), specificity (true negative rate), and F1-score. Ten-fold cross-validation was performed on the training set to assess model stability and select hyperparameters. For aggregate performance assessment, leave-one-out cross-validation (LOOCV) was performed across all 44 patients (21 Engel Class 1, 23 Engel Class 2-4). In LOOCV, each patient was iteratively held out as a single-sample test set while the model was trained on the remaining 43 patients. Predictions were aggregated across all folds to compute overall performance metrics. Odds ratios and 95% confidence intervals were computed from the exponentiated coefficients.

Declarations

- **Funding:** This work was supported by NIH R35-NS132228 (to S.V.S.) and NIH R01NS125897 (to J.-Y.K.).
- **Conflict of interest:** S.V.S. is President and Co-Founder of NeuroLogic Solutions. G.K. is Director of Software Development of NeuroLogic Solutions. The authors declare no other competing interests.
- **Ethics approval and consent to participate:** All data were acquired with the approval of the local Institutional Review Board (IRB) at each clinical institution: Cleveland Clinic by the Cleveland Clinic Institutional Review Board, Johns Hopkins

Table 1 Summary of Patient Demographics and Clinical Characteristics

Characteristic	CC	JHH	NIH	UPMC	Total
Number of Patients	27	4	8	5	44
Sex (Male/Female)	13/14	2/2	6/2	3/2	24/20
Age Range (years)	16–65	24–62	16–46	23–46	16–65
Surgical Outcome					
Engel Class 1 (Success)	11	3	4	3	21
Engel Class 2–4 (Failure)	16	1	4	2	23
MRI Findings					
Normal	24	0	4	4	32
Abnormal	3	4	4	1	12

CC = Cleveland Clinic; JHH = Johns Hopkins Hospital; NIH = National Institutes of Health; UPMC = University of Pittsburgh Medical Center. Surgical outcomes were assessed at $\geq$12 months postoperatively using the Engel Surgical Outcome Scale. Success was defined as Engel Class 1 (free of disabling seizures).

Table 2 Logistic Regression Model Coefficients

Feature	Coefficient	Std. Error	z-statistic	p-value
EZ Tail Proportion	1.59	0.50	3.20	0.0014
Intercept	–0.044	0.37	–0.12	0.91

Logistic regression coefficients for predicting Engel Class 1 outcome. Final model trained on data from all 44 patients. Positive coefficients indicate that higher EZ tail proportion values are associated with increased probability of surgical success.

Hospital by the Johns Hopkins IRB (Protocol Number: NA_00009990; Principal Investigator: Joon Kang), National Institutes of Health by the National Institutes of Health IRB, and University of Pittsburgh Medical Center by the University of Pittsburgh Medical Center IRB. Informed consent was obtained at each clinical center. The acquisition of data for research purposes was completed with no impact on the clinical objectives of the patient stay. Digitized data were stored in an IRB-approved database compliant with Health Insurance Portability and Accountability Act (HIPAA) regulations.

- **Consent for publication:** Not applicable. The data presented in this manuscript are de-identified and aggregated; no tpersonally identifiable information, images, or videos are included.
- **Data availability:** Deidentified iEEG data reported in this study cannot be deposited in a public repository due to patient privacy restrictions. Data may be available upon reasonable request to S.V.S., subject to institutional data sharing agreements.
- **Code availability:** All original code for dynamic network model estimation, virtual resection analysis, and statistical modeling has been deposited at [GitHub repository to be provided upon publication] and is publicly available as of the date of publication.

- **Author contribution:** Conceptualization, S.V.S.; Methodology, D.W. and S.V.S.; Software, D.W.; Formal Analysis, D.W.; Investigation, D.W. and S.V.S.; Data Curation, K.M.G.; Visualization, D.W. and S.V.S.; Writing – Original Draft, D.W., E.A.P., G.K., and S.V.S.; Writing – Review & Editing, D.W., E.A.P., G.K., V.B., J.-Y.K., J.G.-M., and S.V.S.; Supervision, S.V.S.; Project Administration, S.V.S.; Funding Acquisition, S.V.S. and J.-Y.K.

Acknowledgements. The authors thank the clinical teams at Cleveland Clinic, Johns Hopkins Hospital, National Institutes of Health, and University of Pittsburgh Medical Center for their contributions to data collection and clinical annotation.

References

[1] Fiest, K. M. *et al.* Prevalence and incidence of epilepsy: A systematic review and meta-analysis of international studies. *Neurology* **88**, 296–303 (2017).

[2] Kwan, P. *et al.* Definition of drug resistant epilepsy: consensus proposal by the ad hoc task force of the ILAE commission on therapeutic strategies. *Epilepsia* **51**, 1069–1077 (2010).

[3] Berg, A. T. *et al.* How long does it take for epilepsy to become intractable? a prospective investigation. *Annals of Neurology* **60**, 73–79 (2006).

[4] Sinha, N. *et al.* Intracranial EEG structure-function coupling and seizure outcomes after epilepsy surgery. *Neurology* **101**, e1293–e1306 (2023). URL https://www.neurology.org/doi/full/10.1212/WNL.0000000000207661. Publisher: Wolters Kluwer.

[5] Gallagher, R. S. *et al.* The sixth sense: how much does interictal intracranial EEG add to determining the focality of epileptic networks? *Brain Communications* **6**, fcae320 (2024). URL https://doi.org/10.1093/braincomms/fcae320.

[6] Lüders, H. O., Najm, I., Nair, D., Widdess-Walsh, P. & Bingman, W. The epileptogenic zone: general principles. *Epileptic Disorders* (2006).

[7] Bernabei, J. M. *et al.* Quantitative approaches to guide epilepsy surgery from intracranial EEG. *Brain* **146**, 2248–2258 (2023). URL https://doi.org/10.1093/brain/awad007.

[8] Jobst, B. C. & Cascino, G. D. Resective epilepsy surgery for drug-resistant focal epilepsy: A review. *JAMA* **313**, 285–293 (2015). URL https://doi.org/10.1001/jama.2014.17426.

[9] Malmgren, K. & Edelvik, A. Long-term outcomes of surgical treatment for epilepsy in adults with regard to seizures, antiepileptic drug treatment and employment. *Seizure - European Journal of Epilepsy* **44**, 217–224 (2017). URL https://www.seizure-journal.com/article/S1059-1311(16)30183-2/fulltext. Publisher: Elsevier.

[10] Litt, B. *et al.* Epileptic seizures may begin hours in advance of clinical onset: A report of five patients. *Neuron* **30**, 51–64 (2001). URL https://www.cell.com/neuron/abstract/S0896-6273(01)00262-8. Publisher: Elsevier.

[11] Rosenow, F. & Lüders, H. Presurgical evaluation of epilepsy. *Brain* **124**, 1683–1700 (2001). URL https://doi.org/10.1093/brain/124.9.1683.

[12] Gliske, S. V. *et al.* Universal automated high frequency oscillation detector for real-time, long term EEG. *Clinical Neurophysiology* **127**, 1057–1066 (2016). URL https://www.sciencedirect.com/science/article/pii/S1388245715007257.

[13] Nariai, H. *et al.* Prospective observational study: Fast ripple localization delineates the epileptogenic zone. *Clinical Neurophysiology* **130**, 2144–2152 (2019). URL https://www.sciencedirect.com/science/article/pii/S1388245719312192.

[14] Park, C. J. & Hong, S. B. High frequency oscillations in epilepsy: Detection methods and considerations in clinical application. *Journal of Epilepsy Research* **9**, 1–13 (2019). URL https://pmc.ncbi.nlm.nih.gov/articles/PMC6706641/.

[15] Kramer, M. A. & Cash, S. S. Epilepsy as a disorder of cortical network organization. *The Neuroscientist : a review journal bringing neurobiology, neurology and psychiatry* **18**, 360–372 (2012). URL https://pmc.ncbi.nlm.nih.gov/articles/PMC3736575/.

[16] Myers, P. *et al.* Diagnosing epilepsy with normal interictal EEG using dynamic network models. *Annals of Neurology* **97**, 907–918 (2025). URL https://onlinelibrary.wiley.com/doi/abs/10.1002/ana.27168. _eprint: https://onlinelibrary.wiley.com/doi/pdf/10.1002/ana.27168.

[17] Gunnarsdottir, K. M. *et al.* Source-sink connectivity: a novel interictal EEG marker for seizure localization. *Brain* **145**, 3901–3915 (2022). URL https://doi.org/10.1093/brain/awac300.

[18] Roy, S. *et al.* Eigenvector biomarker for prediction of epileptogenic zones and surgical success from interictal data. *Frontiers in Network Physiology* **5** (2025). URL https://www.frontiersin.org/journals/network-physiology/articles/10.3389/fnetp.2025.1565882/full. Publisher: Frontiers.

[19] Hespanha, J. P. *Linear Systems Theory* (Princeton Press, Princeton, New Jersey, 2018). ISBN13: 9780691179575.

[20] Kini, L. G. *et al.* Virtual resection predicts surgical outcome for drug-resistant epilepsy. *Brain: A Journal of Neurology* **142**, 3892–3905 (2019).

[21] Nissen, I. A. *et al.* Optimization of epilepsy surgery through virtual resections on individual structural brain networks. *Scientific Reports* **11**, 19025 (2021). URL https://www.nature.com/articles/s41598-021-98046-0. Publisher: Nature

693 Publishing Group.

694 [22] Demuru, M. *et al.* Validation of virtual resection on intraoperative interic-
695 tal data acquired during epilepsy surgery. *Journal of Neural Engineering* **17**,
696 066002 (2020). URL https://dx.doi.org/10.1088/1741-2552/abc3a8. Publisher:
697 IOP Publishing.

698 [23] Li, C., Su, H. & Liu, Y. Predicting surgical outcome in patients with drug-
699 resistant epilepsy using autoregressive connectivity and virtual resection. *IEEE*
700 *Journal of Biomedical and Health Informatics* **29**, 2199–2209 (2025). URL https:
701 //ieeexplore.ieee.org/document/10772327.

702 [24] Kalitzin, S., Petkov, G., Demuru, M. & Widman, G. *Prospecting epilepsy surgery*
703 *outcome using virtual resection paradigm. computational-model validation.* 2020
704 IEEE Conference on Computational Intelligence in Bioinformatics and Computa-
705 tional Biology (CIBCB), 1–8 (2020). URL https://ieeexplore.ieee.org/document/
706 9277710.

707 [25] Sun, J. *et al.* Virtual resection evaluation based on sEEG propagation network
708 for drug-resistant epilepsy. *Scientific Reports* **14**, 25542 (2024). URL https:
709 //www.nature.com/articles/s41598-024-77216-w. Publisher: Nature Publishing
710 Group.

711 [26] Goodfellow, M. *et al.* Estimation of brain network ictogenicity predicts outcome
712 from epilepsy surgery. *Scientific Reports* **6**, 29215 (2016). URL https://www.
713 nature.com/articles/srep29215. Publisher: Nature Publishing Group.

714 [27] Jirsa, V. *et al.* Personalised virtual brain models in epilepsy. *The Lancet Neu-*
715 *rology* **22**, 443–454 (2023). URL https://linkinghub.elsevier.com/retrieve/pii/
716 S147444222300008X.

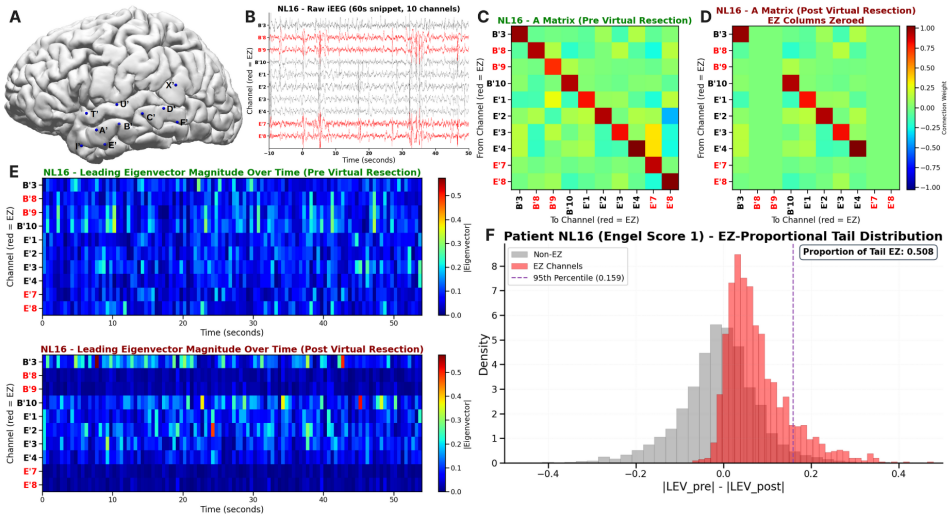

Fig. 1 Virtual Resection Pipeline for LEV-Based Surgical Outcome Prediction. Schematic overview of the computational pipeline for predicting surgical outcomes using leading eigenvector (LEV) analysis and virtual resection. **(A) Intracranial EEG Acquisition.** Stereo-electroencephalography (sEEG) electrodes are implanted according to clinical presurgical hypotheses. Raw intracranial EEG signals are recorded during interictal periods (at least 1 hour from any seizure event) at sampling rates of 500 Hz to 2 kHz. The clinical team annotates channels corresponding to the epileptogenic zone (EZ) based on ictal onset patterns and seizure semiology. EZ channels are color-coded in red. **(B) Signal Preprocessing and Segmentation.** Raw iEEG signals undergo bandpass filtering (0.5–300 Hz), notch filtering at 60 Hz and harmonics, and common average referencing. Preprocessed signals are segmented into non-overlapping 500 ms windows for model estimation. Channels not recording from gray matter or exhibiting excessive noise are excluded. **(C) Dynamic Network Model Estimation.** For each 500 ms window, a linear time-invariant state-transition matrix A is estimated using least squares regression, where $x(t+1) = Ax(t)$ describes how each channel's activity at time t influences all channels at time $t+1$. The matrix element A_{ij} quantifies the directed influence of channel j on channel i. Only matrices with $R^2 > 0.6$ are retained. **(D) Virtual Resection.** The columns of A corresponding to EZ channels are set to zero, eliminating their outgoing influence on the network. **(E) Leading Eigenvector Computation.** The leading eigenvector (LEV) of each A matrix (for both resected and non-resected) is computed, representing the steady-state distribution of network activity. Channels with high LEV magnitude correspond to network "sinks" that accumulate influence from other regions. The change in LEV magnitude ($\Delta\text{LEV} = |\text{LEV}_{pre}| - |\text{LEV}_{post}|$) quantifies the effect of simulated EZ removal on each channel's network influence. **(F) Feature Extraction and Outcome Prediction.** All ΔLEV values are pooled across time windows and channels. The EZ tail proportion is computed as the fraction of elements in the top 5% of the ΔLEV distribution that originate from EZ channels. This scalar feature is used in logistic regression to predict surgical outcome (Engel Class 1 vs. Engel Class 2–4). Each distribution (EZ and Non-EZ) is independently normalized so that its total area equals 1, allowing visual comparison of distribution shapes regardless of sample sizes.

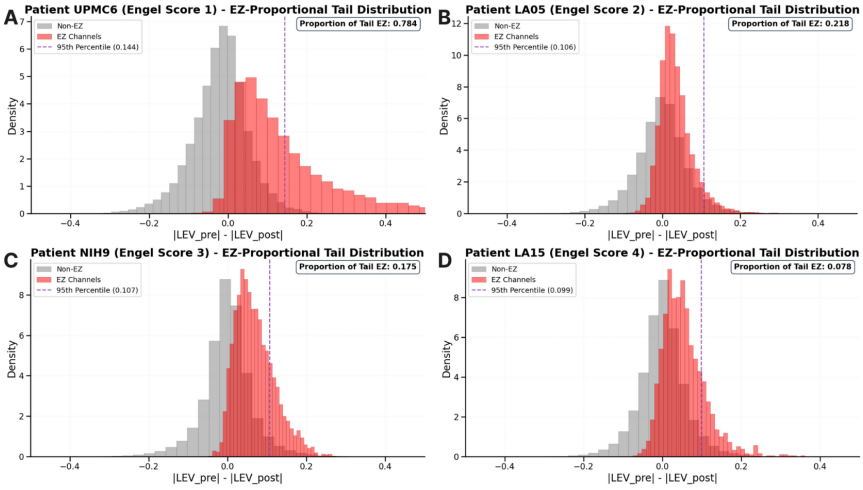

Fig. 2 Distribution of ΔLEV Values Across Patients Grouped by Engel Score. Representative histograms showing the distribution of $\Delta\text{LEV} = |\text{LEV}_{pre}| - |\text{LEV}_{post}|$ computed across all time windows and channels for individual patients. Positive values indicate reduction in eigenvector magnitude following virtual resection. The purple dashed line marks the patient-specific upper 5% quantile threshold. Red indicates elements from EZ-labeled channels and grey depicts non-EZ elements. A kernel density estimation curve (gray) overlays each histogram. The y-axis shows probability density, where each distribution (EZ and Non-EZ) is independently normalized so that its total area equals 1. This allows visual comparison of the distribution shapes regardless of the different sample sizes between EZ and Non-EZ channels. The annotation in each panel reports the proportion of tail mass attributable to EZ elements. Panels are grouped by Engel score (1–4), with patient identifiers colored by outcome **(A)** Engel 1 = seizure free; **(B-D)** Engel 2–4 = ongoing seizures. Patients achieving seizure freedom (Engel Class 1) show substantially higher EZ tail proportions compared to those with poor outcomes. Patients with worse outcomes (higher Engel scores) have progressively less of their 5% quantile threshold consisting of EZ channels.

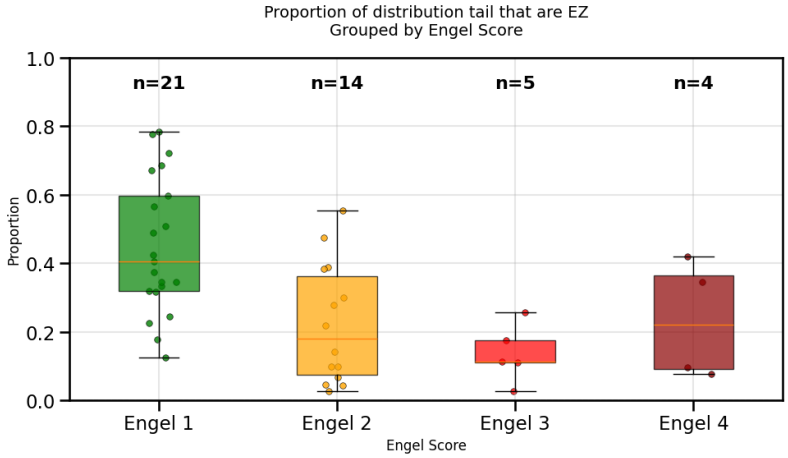

Fig. 3 EZ Tail Proportion Stratified by Engel Outcome Score. Box plots showing the distribution of EZ tail proportion values within each Engel outcome class. The EZ tail proportion is defined as the fraction of elements in the top 5% of the ΔLEV distribution that originate from clinically annotated EZ channels. Individual patients are shown as scattered points, with sample sizes annotated above each box. Box plots display median, interquartile range, and whiskers extending to 1.5× IQR. Higher proportions indicate stronger effects of virtual resection on EZ channel network influence. Engel Class 1 patients (seizure free) exhibit significantly higher EZ tail proportions compared to Engel Class 2–4 patients (ongoing seizures), supporting the use of this metric as a predictive biomarker.

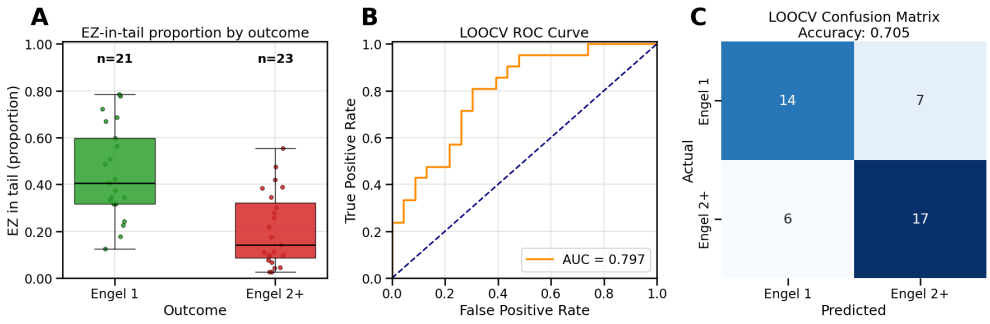

Fig. 4 Machine Learning Model Performance for Surgical Outcome Prediction. Evaluation of the logistic regression classifier using EZ tail proportion to predict surgical outcomes. **(A)** Box plots showing EZ tail proportion values in the training cohort ($n = 44$) stratified by outcome, with individual patients shown as jittered points and sample sizes annotated. Higher values are associated with Engel Class 1 outcomes. **(B)** Receiver operating characteristic (ROC) curve from leave-one-out cross-validation (LOOCV; $n = 44$), demonstrating discrimination between Engel Class 1 and Engel Class 2–4 outcomes (AUC = 0.8). Each prediction represents an out-of-sample probability estimate where the model was trained on all other patients. The AUC 95% confidence interval derived from 1,000 bootstrap resamples was $0.802 \pm 1.96(0.066)$ or $[0.672, 0.931]$, where 0.802 was the mean of the 1,000 bootstrap resamples and 0.066 was the standard error. The diagonal dashed line indicates chance performance. **(C)** Confusion matrix for the test set showing classification performance: overall accuracy = 71%, specificity = 74%, sensitivity = 67%. True labels are shown on the y-axis; predicted labels on the x-axis.

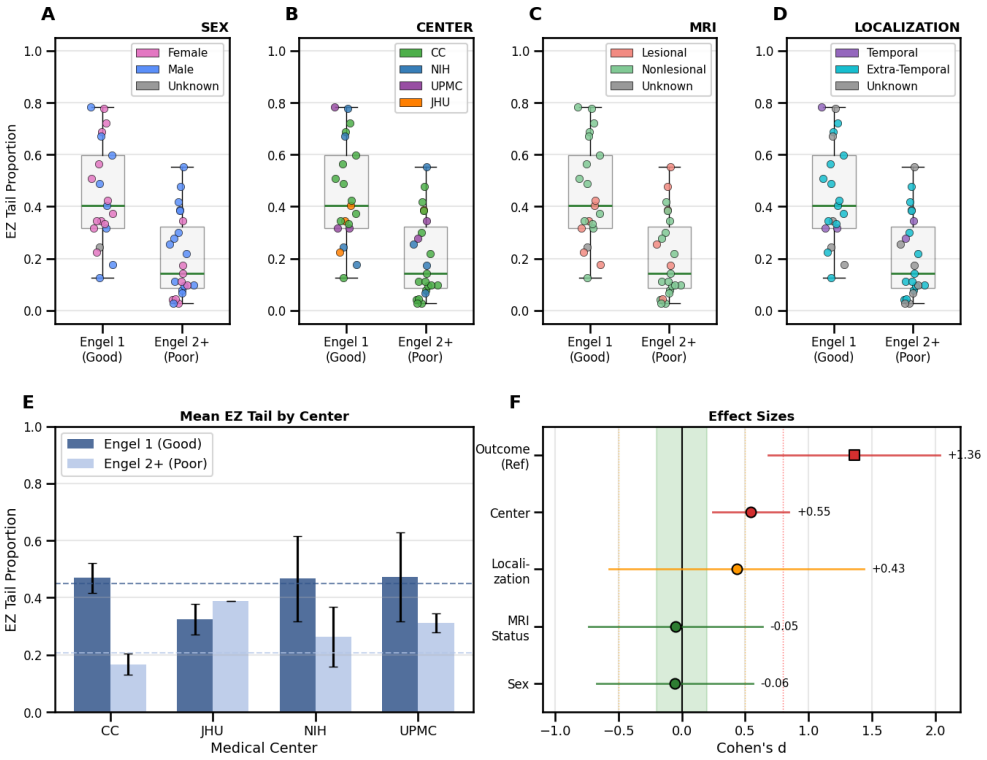

Fig. 5 Robustness of LEV-Based EZ Identification Across Clinical Subgroups. Distribution of EZ tail proportion stratified by surgical outcome (Engel I vs. Engel II+) and colored by clinical covariates, demonstrating the robustness of leading eigenvector (LEV) localization across heterogeneous patient populations. Green horizontal lines indicate group medians. **(A) Sex.** EZ tail proportion distributions show no systematic differences between male and female patients within each outcome group, indicating the LEV metric is not confounded by sex-related differences in brain network organization. **(B) Medical Center.** Distributions are consistent across four independent clinical sites (CC, NIH, UPMC, JHU), demonstrating that LEV-based EZ identification generalizes across different data acquisition systems, electrode configurations, and clinical protocols. **(C) MRI Lesional Status.** Patients with MRI-positive (lesional) and MRI-negative (nonlesional) epilepsy show comparable EZ tail proportion distributions within outcome groups, indicating that LEV localization is effective regardless of whether a structural abnormality is visible on imaging. **(D) Epilepsy Localization.** The metric performs consistently for both temporal lobe epilepsy and extra-temporal epilepsy cases, suggesting broad applicability across different epileptogenic network topologies. **(E) Mean EZ Tail by Center.** Bar chart comparing mean EZ tail proportion (±SEM) between Engel I (good outcome, dark blue) and Engel II+ (poor outcome, light blue) patients across medical centers. Dashed horizontal lines indicate pooled means for each outcome group. The consistent separation between outcome groups across centers supports the generalizability of the LEV metric. **(F) Effect Sizes.** Forest plot displaying Cohen's d effect sizes with 95% confidence intervals for clinical covariates. The green shaded region ($|d| < 0.2$) indicates negligible effect sizes. Sex, MRI status, and localization show negligible effects ($|d| < 0.2$), while center shows a small effect ($d = 0.55$). The reference outcome comparison (Engel I vs. Engel2+) shows a large effect ($d = 1.36$), confirming that surgical outcome—not demographic or clinical confounders—drives the observed differences in EZ tail proportion.